

**Millimeter-Wave and Submillimeter-Wave/Terahertz
Passive Imaging System Requirements: A Phenomenological
Perspective**

by Steven R. Murrill

ARL-TR-6408

May 2013

NOTICES

Disclaimers

The findings in this report are not to be construed as an official Department of the Army position unless so designated by other authorized documents.

Citation of manufacturer's or trade names does not constitute an official endorsement or approval of the use thereof.

Destroy this report when it is no longer needed. Do not return it to the originator.

Army Research Laboratory

Adelphi, MD 20783-1197

ARL-TR-6408

May 2013

**Millimeter-Wave and Submillimeter-Wave/Terahertz
Passive Imaging System Requirements: A Phenomenological
Perspective**

Steven R. Murrill

Sensors and Electron Devices Directorate, ARL

REPORT DOCUMENTATION PAGE

Form Approved
OMB No. 0704-0188

Public reporting burden for this collection of information is estimated to average 1 hour per response, including the time for reviewing instructions, searching existing data sources, gathering and maintaining the data needed, and completing and reviewing the collection information. Send comments regarding this burden estimate or any other aspect of this collection of information, including suggestions for reducing the burden, to Department of Defense, Washington Headquarters Services, Directorate for Information Operations and Reports (0704-0188), 1215 Jefferson Davis Highway, Suite 1204, Arlington, VA 22202-4302. Respondents should be aware that notwithstanding any other provision of law, no person shall be subject to any penalty for failing to comply with a collection of information if it does not display a currently valid OMB control number.

PLEASE DO NOT RETURN YOUR FORM TO THE ABOVE ADDRESS.

1. REPORT DATE (DD-MM-YYYY) May 2013		2. REPORT TYPE Final		3. DATES COVERED (From - To) 02/2013 to 03/2013	
4. TITLE AND SUBTITLE Millimeter-Wave and Submillimeter-Wave/Terahertz Passive Imaging System Requirements: A Phenomenological Perspective				5a. CONTRACT NUMBER	
				5b. GRANT NUMBER	
				5c. PROGRAM ELEMENT NUMBER	
6. AUTHOR(S) Steven R. Murrill				5d. PROJECT NUMBER	
				5e. TASK NUMBER	
				5f. WORK UNIT NUMBER	
7. PERFORMING ORGANIZATION NAME(S) AND ADDRESS(ES) U.S. Army Research Laboratory ATTN: RDRL-SEE-E 2800 Powder Mill Road Adelphi, MD 20783-1197				8. PERFORMING ORGANIZATION REPORT NUMBER ARL-TR-6408	
9. SPONSORING/MONITORING AGENCY NAME(S) AND ADDRESS(ES)				10. SPONSOR/MONITOR'S ACRONYM(S)	
				11. SPONSOR/MONITOR'S REPORT NUMBER(S)	
12. DISTRIBUTION/AVAILABILITY STATEMENT Approved for public release; distribution unlimited.					
13. SUPPLEMENTARY NOTES					
14. ABSTRACT The phenomenology of imaging in the millimeter-wave (MMW) and submillimeter-wave (SMMW)/terahertz (THz) frequency regimes is investigated and described. The primary factors related to imaging in these frequency regimes are phenomenologically driven and involve trade-offs between spatial (angular) resolution; the impact of atmospheric and obscurant attenuations such as fog, dust, and concealing materials; and system sensitivity requirements. Minimum system sensitivity requirements for adequate imaging in three important military/security scenarios are identified and described in terms of minimum apparent temperature differences between targets and their backgrounds. Mathematical equations for calculating the minimum system sensitivity (noise equivalent power [NEP] per root hertz [Hz]) required to provide image frames with enough signal-to-noise ratio (SNR) to produce good imagery at video frame rates are derived.					
15. SUBJECT TERMS Millimeter-Wave, Sub-Millimeter-Wave, Terahertz, Imaging System, Phenomenology, Apparent Brightness Temperature, Contrast Ratio, SNR, SCR					
16. SECURITY CLASSIFICATION OF:			17. LIMITATION OF ABSTRACT UU	18. NUMBER OF PAGES 32	19a. NAME OF RESPONSIBLE PERSON Steven R. Murrill
a. REPORT Unclassified	b. ABSTRACT Unclassified	c. THIS PAGE Unclassified			19b. TELEPHONE NUMBER (Include area code) (301) 394-5210

Contents

List of Figures	iv
List of Tables	iv
1. Introduction	1
2. Imaging Phenomenology	2
2.1 Atmospheric Effects	2
2.2 Other Obscurant Effects	3
2.3 Sky Illumination	7
2.4 Target/Background Reflectivities and Emissivities	8
2.5 Spatial Resolution.....	10
3. Imaging Regimes and Scenarios	12
3.1 Scenario A: In-flight Obstacle Avoidance	12
3.2 Scenario B: Landing/Takeoff Obstacle Avoidance.....	13
3.3 Scenario C: Concealed Weapon Detection/Identification.....	14
4. Imaging System Requirements	15
5. Discussion and Conclusions	20
6. References	23
List of Symbols, Abbreviations, and Acronyms	25
Distribution List	26

List of Figures

Figure 1. Attenuation (dB/km) across the electromagnetic spectrum at sea level based on currently accepted models. Rain = 4 mm/hr, fog = 100 m visibility, STD (standard atmosphere) = 7.5 gm/m ³ water vapor, and 2XSTD = 15 gm/m ³ water vapor (excerpted from Rosker et al. [1, 3]).	2
Figure 2. Atmospheric attenuation (dB/km) at sea level pressures for five different conditions of temperature, humidity, and atmospheric particulates (excerpted from Rosker et al. [1]).	3
Figure 3. Dynamic W-band dust cloud attenuation setup at Yuma Proving Ground (YPG) used to measure the attenuation due to dust clouds for small, medium, and large, rotary aircraft (excerpted from Mackrides et al. [6]).	4
Figure 4. Plot of attenuation within the W-band during the rotary craft flyovers (excerpted from Mackrides et al. [6]).	4
Figure 5. THz and mid-IR transmission through eight clothing samples with a common vertical axis (and scale) but broken horizontal axis (and different frequency scales) (excerpted from Bjarnason et al. [7]).	6
Figure 6. Transmission properties of a variety of clothing (excerpted from Petkie et al. [8]).	7
Figure 7. Apparent radiometric sky temperature corresponding to the sea level conditions shown in table 1 (excerpted from Rosker et al. [1]).	7
Figure 8. Illustration of the radiometric model for passive target/background thermal emission.	15
Figure 9. Spectral exitance of a blackbody at a temperature of 300 K.	17
Figure 10. Spectral exitance of a blackbody at a temperature of 300 K plotted on a log-log scale.	18

List of Tables

Table 1. Characteristics of weather conditions used in figures 1 and 2.	3
Table 2. Optical properties of 5-mm-thick explosives, skin, metal, denim, and T-shirt (excerpted from Appleby et al. [2]).	9
Table 3. Mean nadir emissivities for video classifications (excerpted from Hewison [11]).	9
Table 4. Limiting spatial resolution as a function of operating frequency for a fixed imaging system aperture diameter of 0.5 m.	10
Table 5. Maximum range that an imaging system can be used to perform the task of detecting a target within a background for a range of EM radiation frequencies.	11

1. Introduction

Renewed interest and investment in millimeter-wave (MMW) (millimeter wavelength (λ)—nominally 30 GHz [$\lambda = 10$ mm] to 300 GHz [$\lambda = 1$ mm]) and submillimeter-wave (SMMW)/terahertz (THz) (*submillimeter* wavelength—nominally 0.3 THz [$\lambda = 1$ mm] to 3 THz [$\lambda = 0.1$ mm]) imaging technology has increased in recent years. Demand for imaging in degraded visual environments (DVEs) and for imaging concealed weaponry carried by people in both the domestic and theater-of-operations realms is on the increase. Currently, MMW imaging technology has demonstrated the potential to image through such obscurants as atmospheric fog, smoke, blowing dust, and sand (brownout); and concealment materials such as clothing. SMMW/THz imaging technology also offers the potential to image through these obscurants, but with higher spatial resolution for a given imaging system aperture size, allowing the potential for target/weapon detection or identification at greater, more-useful (safer) standoff ranges.

Many MMW and SMMW/THz imaging system approaches are now being investigated including active-illumination-based systems, passive-illumination/emission-based systems, continuous-wave (CW) systems, and time-domain (active, pulsed) systems. Typical system architectures include focal-plane-array (FPA), scanning line-array, and single-pixel scanning receiver (and possibly transmitter) sub-systems. In general, active-illumination imaging systems are more complex than passive (CW) imaging systems, but offer the potential to produce imagery with better target-to-background contrast ratios (CRs) and better signal-to-noise ratios (SNRs). Concurrently, active-illumination-based systems typically produce imagery that is more specular in nature, which can also be degraded by clutter from illumination backscatter. Passive-illumination-based systems are dependent on both natural/environmental illumination and target/background emissions, but typically produce imagery that is less specular and more natural in appearance.

This report focuses on *passive* MMW and SMMW/THz imaging system requirements that are shaped and driven by the imaging phenomenology. The perspective is that the phenomenology then drives the critical imaging characteristics of apparent target-to-background CRs, system receiver target and background signal (power) levels, and signal (target)-to-clutter ratios (SCRs). As such, the system receiver characteristics combined with the phenomenology drive the system signal-to-noise plus clutter ratios (SNCRs). This report compares and contrasts the MMW and SMMW/THz imaging regimes, and explores three important imaging scenarios: in-flight obstacle avoidance, landing/takeoff obstacle avoidance, and concealed weapon detection/identification. While many *passive* MMW and SMMW/THz imaging systems have been constructed throughout the United States (and the world) that can produce high-quality, reasonable-contrast, and low-noise imagery given adequate frame times of seconds to minutes, few *passive* systems are capable of producing useful imagery at real-time video rates (nominally

30 Hz). This report draws conclusions about the critical receiver sensitivity levels required to provide useful, real-time (video rate) *passive* imagery in the scenarios explored.

2. Imaging Phenomenology

Several phenomenological effects shape and impact the ability to image objects/targets of interest in the MMW and SMMW/THz frequency regimes. Following is a brief synopsis of the primary factors involved.

2.1 Atmospheric Effects

The primary impact of the atmosphere on MMW and SMMW/THz imaging is attenuation, principally due to water vapor, and scattering from atmospheric particles (1, 2). Figures 1 and 2 (from Rosker et al. [1, 3]) plot atmospheric attenuation as a function of frequency over different ranges. Table 1 lists the atmospheric conditions plotted in figures 1 and 2. Both plots show that atmospheric attenuation increases significantly from approximately 100 GHz to 10 THz with windows of relatively low attenuation. From figure 1, it is interesting to note that in the region of approximately 100 GHz, the atmospheric attenuation is about the same as it is in the 8–12 μm window. Also, note that the primary atmospheric condition that is extremely detrimental to imaging in the visible region is fog, which has little impact in the MMW regime. Figure 2 shows the large variation in atmospheric attenuation for different, normally occurring environmental conditions (1).

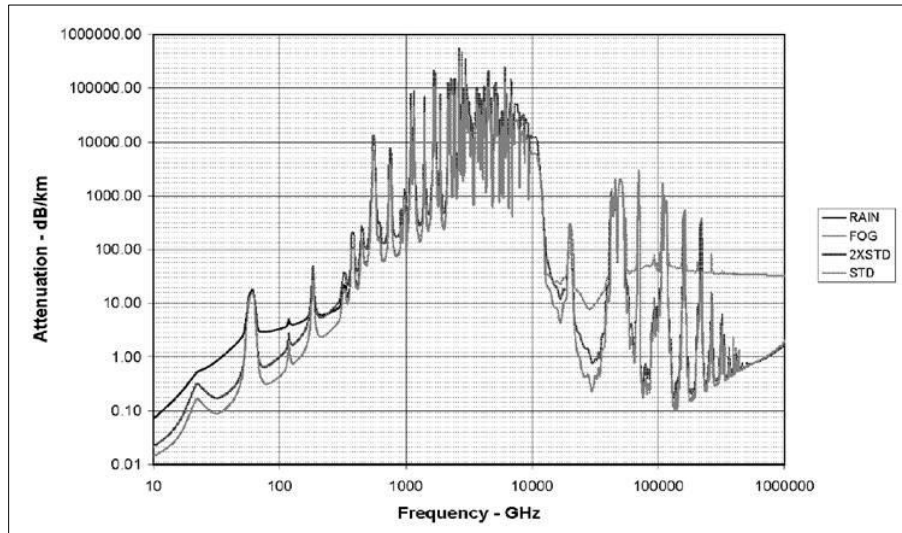


Figure 1. Attenuation (dB/km) across the electromagnetic spectrum at sea level based on currently accepted models. Rain = 4 mm/h, fog = 100 m visibility, STD (standard atmosphere) = 7.5 gm/m^3 water vapor, and 2XSTD = 15 gm/m^3 water vapor (excerpted from Rosker et al. [1, 3]).

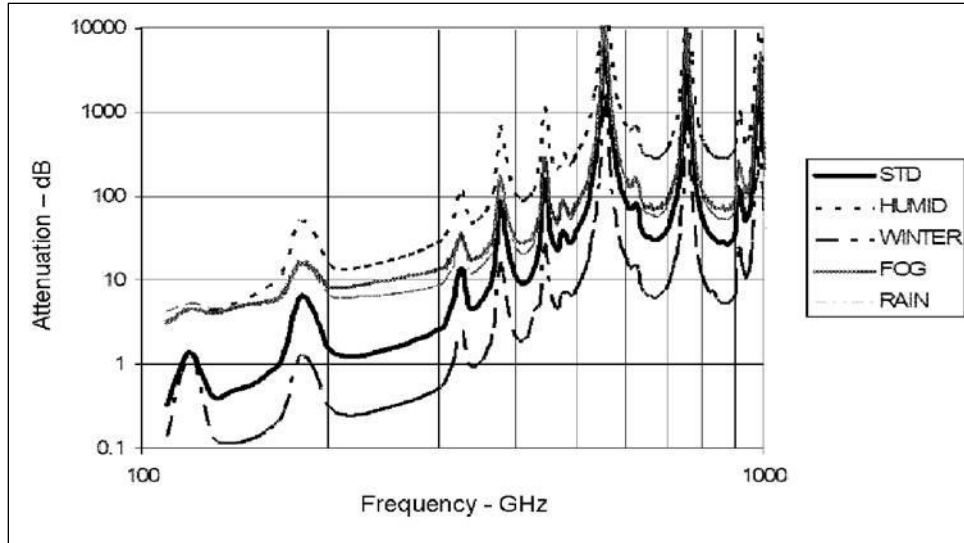


Figure 2. Atmospheric attenuation (dB/km) at sea level pressures for five different conditions of temperature, humidity, and atmospheric particulates (excerpted from Rosker et al. [1]).

Table 1. Characteristics of weather conditions used in figures 1 and 2.

Condition	T (C)	Pres. (Pa)	Rel. Hum.	Rain (mm/hr)	Fog (m)	Dust (m)
STD	20	1013	44%	0	0	0
HHH	35	1013	90%	0	0	0
Winter	-10	1013	30%	0	0	0
Fog	20	1013	44%	0	100	0
Rain	20	1013	44%	4	0	0

The primary impact of the atmosphere on an imaging system's capability to provide imagery useful for detecting or identifying concealed weapons carried by people is the reduction in the SNCR in the sensor image. A lower SNCR can result from reducing the illumination function on the scene (active illumination or sky illumination), reducing the signal reflected or radiated by the scene, or having an intermediate scattering effect. The SNCR is affected by the transmitted power (or the temperature of the surrounding environment in the case of passive imaging); the receiver sensitivity; the reflectivity of the weapon (generally close to one) and skin; and finally the attenuation (or emissivity and reflectivity) of any intervening material, e.g., clothing (1).

Loss from the atmosphere tends to drive system designs to lower frequencies while accepting the loss in resolution or accepting a larger aperture/antenna.

2.2 Other Obscurant Effects

In addition to the atmosphere (primarily fog), other imaging obscurants exist, including dust, smoke, and for the case of imaging concealed weapons carried by people, clothing materials.

Several studies designed to measure the impact of dust on imaging in the MMW regime demonstrate that in heavy dust situations that completely obscure imaging in either the visible or infrared (IR) regimes, there is minimal impact on transmission through dust clouds at MMW lengths, and thus, minimal impact on MMW imaging. In one study, Wikner measured losses less than 0.02 and 0.08 dB for 94 and 217 GHz, respectively, across 1 m of dust with a density of 3000 mg/m^3 (4). In a second study, Schuetz et al. measured an average attenuation of 1.14 dB/km at 77 GHz through a dust cloud created from slow flyovers by a small military helicopter (5). In a third experiment, Mackrides et al. measured a peak attenuation of approximately 20% (0.97 dB) at 77 GHz through a dust cloud created from slow flyovers by a large, heavy military helicopter (6). Figure 3 illustrates the dust cloud attenuation measurement setup for this third experiment. Figure 4 shows a plot of W-band (77 GHz) attenuation during the rotary craft flyovers.

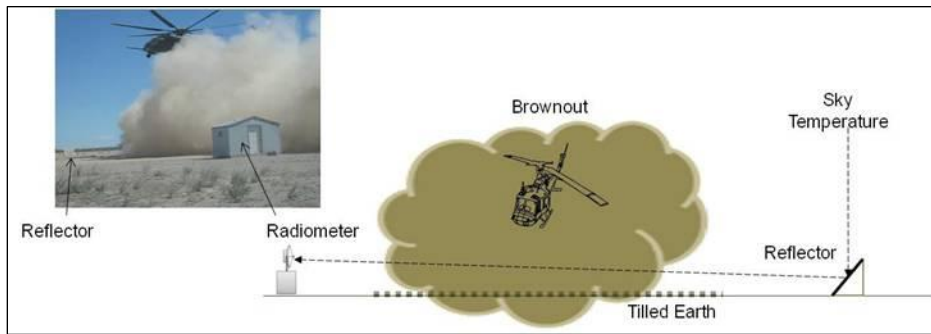


Figure 3. Dynamic W-band dust cloud attenuation setup at Yuma Proving Ground (YPG) used to measure the attenuation due to dust clouds for small, medium, and large rotary aircraft (excerpted from Mackrides et al. [6]).

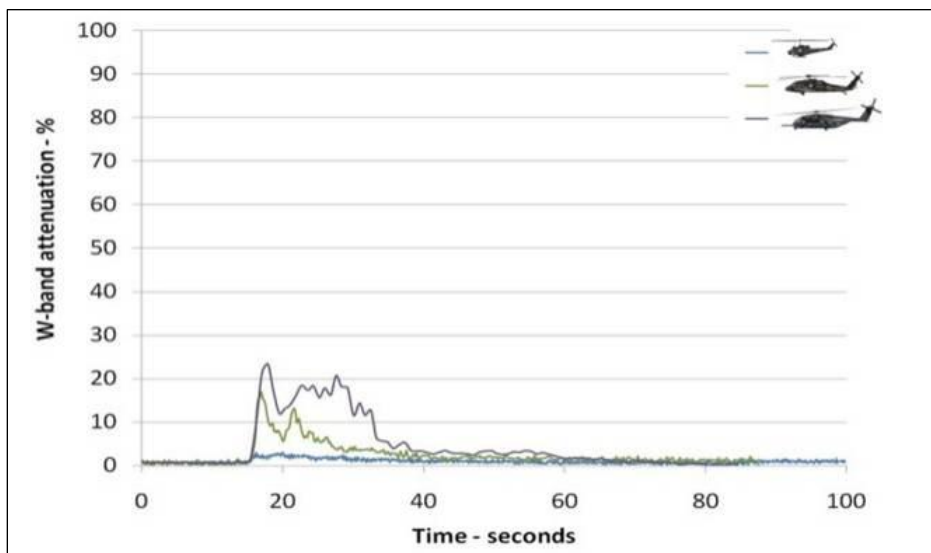


Figure 4. Plot of attenuation within the W-band during the rotary craft flyovers (excerpted from Mackrides et al. [6]).

Attenuation from smoke in the MMW and most of the SMMW/THz imaging regimes will be minimal, as the particle size of smoke is significantly smaller than MMWs.

Studies on the impact of clothing material on the attenuation of MMW and SMMW/THz electromagnetic (EM) radiation show a strong dependence on frequency, material type, and material thickness. One study by Bjarnason et al. that performed transmission measurements on cloth samples from eight types of fabric common in garments and baggage found the following:

- Transmission measurements revealed that all clothing samples were adequately transparent at MMW frequencies up to approximately 300 GHz (based on a 3-dB criterion).
- At frequencies near 1 THz, the average transmission was down by approximately 8 dB with an approximately 9-dB spread.
- Attenuation in the IR region was very high (approximately 25 dB) for all sample types except rayon and nylon (~12 dB of attenuation). The significantly higher transmission through rayon and nylon is attributed to pores intrinsic to these materials.
- Surface backscattering was not measured; however, microphotographs reveal roughness on the scale comparable to a THz wavelength, particularly in the coarse filamentary pattern of nylon and the interlaced weave of rayon and silk. Because these three sample types were found to be the most transparent, it is surmised that any surface scattering must be fairly weak (7).

Figure 5 shows a plot of the results.

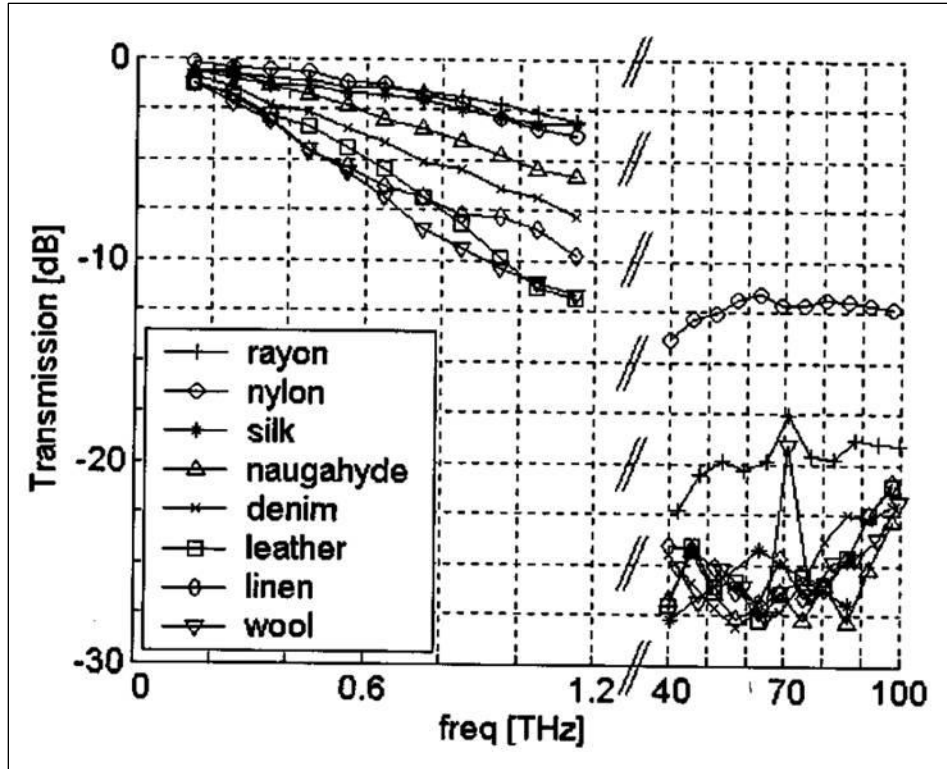


Figure 5. THz and mid-IR transmission through eight clothing samples with a common vertical axis (and scale) but broken horizontal axis (and different frequency scales) (excerpted from Bjarnason et al. [7]).

Another study on the impact of clothing material on the attenuation of MMW and SMMW/THz EM radiation by Petkie et al. measured similar results and found the following:

- Static transmission results through 13 different single-layer clothing items indicate transmission levels greater than 50% from approximately 100 to 600 GHz.
- Dynamic transmission results through an overcoat that was slowly “waved” to mimic the motion of clothing on a moving person show a variation on the order $\pm 10\%$. It is speculated that this level of variation may also be present as a spatial modulation across a static target and that this “clutter” may present more of a limitation to imaging systems than the loss of signal intensity.
- Coherent effects in the clothing material were observed by varying the angle of incidence of the radiation beam. Variations in transmission on the order of approximately 12% were observed as a function of incident radiation angle.
- Active imaging at 640 GHz yielded high resolution and contrast, but also showed coherent effects that can lead to fringes in the images (8).

Figure 6 shows a plot of the results.

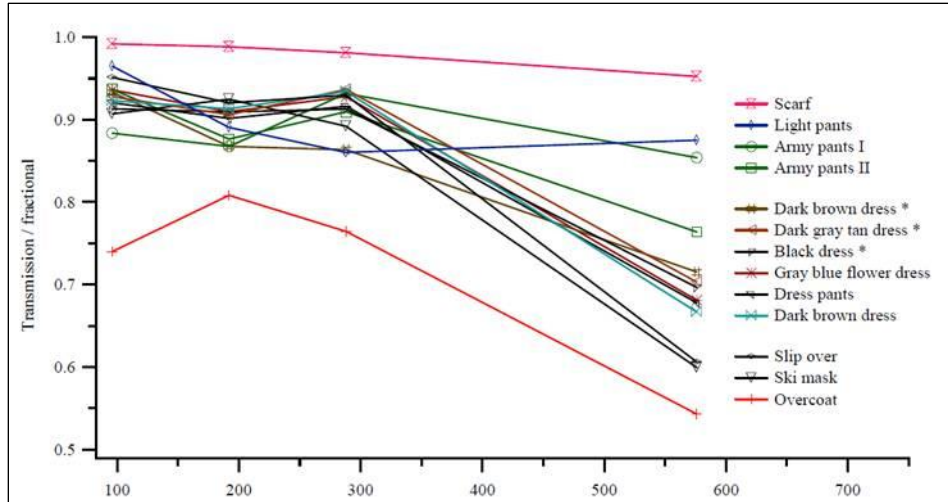


Figure 6. Transmission properties of a variety of clothing (excerpted from Petkie et al. [8]).

2.3 Sky Illumination

For passive MMW imaging systems, where the reflectivities of many objects are relatively high and the wavelengths of the propagating EM radiation are typically substantially longer than the surface roughness of many objects of interest, the apparent sky temperature is an important consideration for detecting objects with different reflectivities. The sky temperature can either enhance the apparent signature of highly reflective items, such as metal weapons (if the imaging geometry is correctly oriented), or it can create an apparent or confusing element in the scene, such as when reflective clothing or skin obscures the detection of weapons (*1*). Figure 7 (from Rosker et al.) plots the apparent sky temperature as a function of frequency.

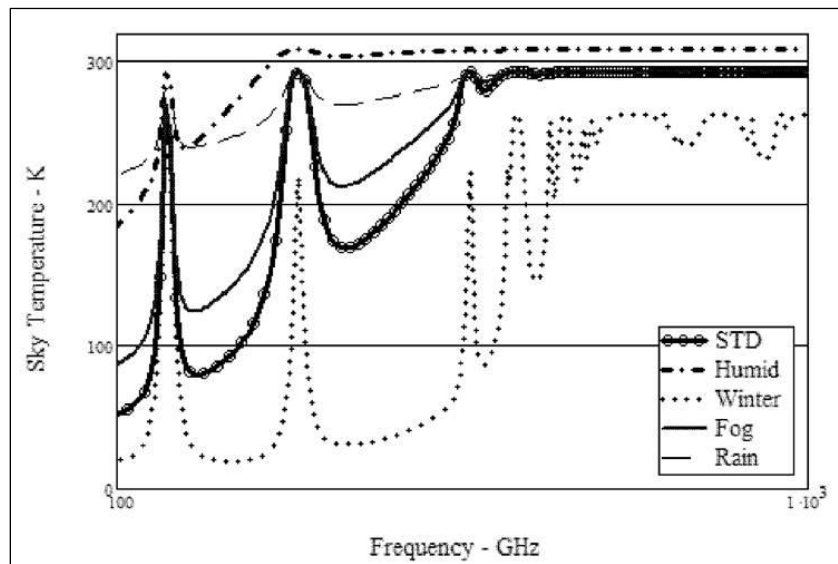


Figure 7. Apparent radiometric sky temperature corresponding to the sea level conditions shown in table 1 (excerpted from Rosker et al. [1]).

Note that while passive MMW systems operating at, say, 94 GHz may be designed to exploit the sky as an illuminator, the available contrast rapidly diminishes as frequency increases in all but the driest environmental conditions. Above approximately 300 GHz, the apparent sky temperature is essentially the same as the background (~ 300 K) (1).

The apparent sky temperature is a strong function of angle from zenith, especially under high-attenuation and/or foggy environmental conditions. Generally, the apparent temperature of the sky is the coldest at zenith and can progressively warm to a maximum at the horizon sky. The horizon sky is typically the part of the sky that has the highest brightness temperature because the path attenuation (hence emission) through the atmosphere is the highest in that direction. In fog, the absorption of MMW energy along a path to the horizon is high enough to make its brightness temperature equal to the ambient air temperature (9).

2.4 Target/Background Reflectivities and Emissivities

For *active* imaging, the signature (target-to-background contrast) is determined by small differences in reflectivity across the band. For passive imaging, the contrast mechanism changes as frequency increases. At frequencies of 100 GHz and below, the optical properties of, for example, the body and explosives are dominated by their *reflectivity* and it is the geometry that gives rise to the signature. In *passive* imaging above 100 GHz, the signature is produced by the differences in *emissivity* and *reflectivity* between skin and explosives or metal. At frequencies of 500 GHz and above, the optical properties are dominated by *emissivity* and it is the physical temperatures, along with *emissivities*, which predominately determine the passive signature.

As frequency increases, emissivity increases while both transmission and reflectivity of non-metallic objects tend to decrease. Where emissivity dominates the optical properties, the passive signature becomes more a function of the physical temperatures of the object and background, as in the IR region of the EM spectrum. Table 2 (from Appleby et al.) lists the emissivity, reflectivity, and transmission of various materials relevant to the concealed weapons detection/identification imaging scenario. Note that while the difference in reflectivity at 100 GHz between human skin ($r = 0.35$) and an explosives pack on the skin ($r = 0.24$) will produce enough contrast for detection of the target (explosives pack), above 500 GHz this difference is substantially reduced with skin ($r = 0.09$) and the explosives pack on the skin ($r = 0.05$). The decrease is due primarily to the increase in emissivities (2).

Table 2. Optical properties of 5-mm-thick explosives, skin, metal, denim, and T-shirt (excerpted from Appleby et al. [2]).

	Emissivity (ϵ)			Reflectivity (r)			Transmission (t)		
	100 GHz	500 GHz	1 THz	100 GHz	500 GHz	1 THz	100 GHz	500 GHz	1 THz
Explosive on skin	0.76	0.95	0.94	0.24	0.05	0.06	0	0	0
Metal	0	0	0	1	1	1	0	0	0
Skin	0.65	0.91	0.93	0.35	0.09	0.07	0	0	0
Denim	0.09	0.49	0.85	0.01	0.01	0.05	0.9	0.5	0.1
tee-shirt	0.04	0.2	0.3	0	0	0.05	0.96	0.8	0.65

In another study, image-based reflectivity measurements that were then used to determine the reflectivity of human skin at a wavelength of 10.6 μm (IR regime) yielded emissivity values from the skin on the back side of the hand between 0.9918 and 0.9985 at a wavelength of 10.6 μm (10).

In a third study, airborne measurements of forest and agricultural land surface emissivity at millimeter wavelengths have been obtained over a range of frequencies (20–200 GHz) and viewing angles (approximately 0° to 50°). Emissivities were measured for open water; lake ice; bare soil; frozen soil; open and close stubble and grass; open and close summer and winter forest; and winter conifers. These results are summarized in table 3 (11).

Table 3. Mean nadir emissivities for video classifications (excerpted from Hewison [11]).

Category	$e(24)$	$e(50)$	$e(89)$	$e(157)$
Water 18C	0.443	0.513	0.573	0.668
Water 0C	0.491	0.588	0.657	0.733
Lake Ice	0.908	0.920	0.922	0.925
Bare Soil	0.955	0.967	0.962	0.966
Frozen Soil	0.962	0.982	0.979	0.980
Open Stubble	0.960	0.966	0.962	0.974
Close Stubble	0.953	0.963	0.962	0.974
Open Grass	0.959	0.968	0.961	0.973
Close Grass	0.964	0.967	0.963	0.972
Summer Open Forest	0.983	0.985	0.983	0.990
Summer Close Forest	0.984	0.987	0.985	0.994
Winter Open Forest	0.985	0.986	0.985	0.987
Winter Close Forest	0.987	0.990	0.991	0.993
Winter Open Conifer	0.987	0.989	0.991	0.994
Winter Close Conifer	0.989	0.990	0.992	0.995

Additional observations made by Hewison were as follow:

- Nadir emissivities for all categories were above 0.90 except for open water (~0.4 to 0.7 depending on frequency).
- Emissivity is a strong function of incident viewing angle for lake water and lake ice. Emissivity is a weak function of incident viewing angle for bare soil, close conifers, and all other forests/conditions.

2.5 Spatial Resolution

The limiting spatial angular resolution of an imaging system using a circular focusing element/aperture is given by

$$\theta = \frac{\lambda}{D} \quad (1)$$

where θ is the limiting spatial angular resolution in radians, λ is the wavelength of the propagating EM radiation in meters, and D is the imaging system aperture diameter in meters (12).

Using the well-known relationship between wavelength and frequency,

$$\lambda = \frac{c}{f} \quad (2)$$

where λ is the wavelength in meters, c is the speed of light in meters per second (3.0×10^8 m/s), and f is the frequency in hertz, and substituting equation 2 into equation 1 yields

$$\theta = \frac{c}{fD} \quad (3)$$

where again θ is the limiting spatial angular resolution in radians, c is the speed of light in meters per second (3.0×10^8 m/s), f is the frequency in hertz, and D is the imaging system aperture diameter in meters.

Using equation 3, table 4 shows the amount of spatial resolution that can be achieved by imaging systems operating in different frequency regimes. The calculations are based on a fixed imaging system aperture size of 0.5 m.

Table 4. Limiting spatial resolution as a function of operating frequency for a fixed imaging system aperture diameter of 0.5 m.

EM Radiation Frequency (GHz)	EM Radiation Wavelength (mm)	System Aperture Diameter (m)	Limiting Angular Resolution (milliradians)
100	3.000	0.5	6.000
640	0.469	0.5	0.938
30,000	0.010	0.5	0.020

The number of spatial cycles of resolution across the critical dimension of a target in object space is given by

$$N_{cyc} = \frac{d}{\theta R} \quad (4)$$

where N_{cyc} is the number of spatial cycles of resolution, d is the critical dimension of a target in meters, θ is the limiting spatial angular resolution in radians, and R is the range or distance in meters between the imaging system and the target of interest.

Rearranging equation 4 and substituting equation 3 into equation 4 yields

$$R = \frac{d \cdot f \cdot D}{c \cdot N_{cyc}} \quad (5)$$

where again R is the range or distance in meters, d is the critical dimension of a target in meters, f is the frequency in hertz, D is the imaging system aperture diameter in meters, c is the speed of light in meters per second (3.0×10^8 m/s), and N_{cyc} is the number of spatial cycles of resolution across the critical dimension of a target in object space.

Using equation 5, the maximum range that an imaging system can be used to perform the task of detecting a target within a background is calculated for a range of EM radiation frequencies under the following assumptions:

- the EM radiation frequencies (f 's) are 100, 640, and 30,000 GHz (30 THz, which corresponds to a 10- μ m wavelength),
- the critical dimension (d) of the target is 3 in or approximately 0.076 m,
- the imaging system aperture diameter (D) is 0.5 m,
- the speed of light (c) in meters per second is 3.0×10^8 m/s, and
- the number of cycles on target (N_{cyc}) required to perform the task of detection is 1.0.

Table 5 shows the results.

Table 5. Maximum range that an imaging system can be used to perform the task of detecting a target within a background for a range of EM radiation frequencies.

EM Radiation Frequency (GHz)	EM Radiation Wavelength (millimeters)	System Aperture Diameter (meters)	Critical Target Dimension (meters)	Spatial Cycles on Target (unitless)	Maximum Standoff Range (meters)
100	3.000	0.5	0.076	1.0	12.7
640	0.469	0.5	0.076	1.0	81.1
30,000	0.010	0.5	0.076	1.0	3800.0

The analysis above demonstrates and quantifies the impact that both the EM wave frequency and the imaging system aperture size have on system resolution, and the ability to resolve and detect a target within a background at standoff ranges. Higher EM wave frequencies result in higher spatial resolution that can be used to detect (or identify) targets at greater standoff ranges or reduce the size of the imaging system aperture, or some combination of both. Larger imaging system apertures also result in higher spatial resolution that can be used to detect (or identify) targets at greater standoff ranges, operate at lower EM wave frequencies, or some combination of both.

3. Imaging Regimes and Scenarios

From a phenomenological perspective, *passive* imaging in the MMW and SMMW/THz regions does in fact divide into two general regimes close to their wavelength-based definitions with a transition region in-between. At frequencies of 100 GHz and below, the optical properties (contrast mechanism) of, for example, the human body (skin) (background) and explosive packs (target) are dominated by their *reflectivity* and it is then the illumination/observation geometry that gives rise to the (target-to-background contrast) signature. Between approximately 100 and 500 GHz, there is a contrast mechanism transition region where the (contrast) is produced by the combination and/or differences in *emissivity* and *reflectivity* between the target and background material, e.g., explosives or metal (target) and human skin (background). At frequencies of 500 GHz and above, the contrast mechanism is dominated by *emissivity* and it is the physical temperatures that largely determine the passive (target-to-background contrast) signature.

As frequency increases, emissivity increases while both transmission and reflectivity of non-metallic objects tend to decrease. Again, where emissivity dominates the optical properties, the passive signature becomes more a function of the physical temperature of the objects, as in the IR region of the EM spectrum.

Additional attributes include relatively low atmospheric, dust, smoke, and clothing-obscurant attenuations in the MMW regime, with increasingly higher atmospheric and clothing-obscurant attenuations in the SMMW/THz regime.

The following sections describe the phenomenology and the respective imaging system requirements for three important passive imaging scenarios—two in the MMW regime and one in the SMMW/THz regime.

3.1 Scenario A: In-flight Obstacle Avoidance

In 2004, Wikner performed measurements to explore the use of image processing enhancement techniques to improve passive MMW (93 GHz) imagery for use in aircraft obstacle avoidance. The effort focused on enhancing detectability of two common obstacles, a concrete office

building and a tree line, from the perspective of low-flying aircraft for terrain-following/terrain-avoidance during very challenging, low-visibility, foggy conditions. Wikner made several important observations:

- The quantity that is important for aircraft obstacle avoidance is the difference in brightness temperature between the *horizon* sky and the obstacle.
- The horizon sky is typically the part of the sky that has the highest brightness temperature because the path attenuation (hence emission) through the atmosphere is the highest in that direction. In fog, the absorption of MMW energy along a path to the horizon is high enough to make its brightness temperature equal to the ambient air temperature.
- Building walls usually emit a brightness temperature close to the ambient temperature, unless they have been warmed by direct sunlight. What little energy is reflected toward the sensor does not come from the cold part of the sky, but rather the warm horizon behind the sensor.
- The brightness temperature difference between the horizon sky and a tree line is typically well below zero on cold days, and just above zero on warm, humid, or foggy days. The brightness contrast between the *horizon* sky and a tree line in fog is consistently just a few degrees positive (typically about 2 K), due to the fact that the foggy *horizon* sky has a high brightness temperature compared to the (*cold*) sky temperature reflected off of the leaves or branches of trees in the tree line. (Note that here the leaves and tree branches are the target; more typically, they represent a cluttered background.)
- Finally, the measured data suggest that a thermal sensitivity of about 0.2 K is required for a passive imaging system operating at 30 Hz if it is to be used to reliably detect and avoid collisions with tree lines in foggy conditions (13).

3.2 Scenario B: Landing/Takeoff Obstacle Avoidance

In 2006, Wikner performed measurements to quantify the available brightness temperature contrast between various obstacles that are relevant to helicopter takeoffs and landings in a sand environment. Passive radiometric images (at 93 GHz) of various obstacles situated in a sand background were taken at various depression angles and with vertical and horizontal polarizations. Obstacles included a fence post, a large boulder, a Hedgehog, cinder blocks, a J-log, a chain-link fence, a berm, and a ditch. Key findings from the study include the following:

- There is a strong polarimetric signature/effect present for both sand and cinder block between 10° and 30° of depression angle.
- Measurements of sand at a 30° depression angle led to estimates of effective emissivities for both vertical and horizontal polarizations of 0.86, and 0.78, respectively.

- Most obstacles yielded a brightness temperature contrast of approximately 6 K, with most objects being slightly less bright than the sand background. The wooden fence post, being a good emitter, was at a brighter temperature than the surrounding sand.
- Despite good sensor thermal resolution/sensitivity (<0.3 K), the ditch was barely visible as a dark line across the image. The berm was also very difficult to detect (14).

In 2009, Schuetz et al. (15) performed a series of studies to determine the impact of dust clouds generated by helicopter landings, takeoffs, and hovering. The data were acquired using a W-band (77 GHz), dual-polarization radiometric scanner using optical-upconversion detectors. Key findings from the studies include the following:

- Static, passive MMW images were collected for 23 different landing zone obstacles against a packed dirt background. Calibrated contrast measurements were calculated for six, simple landing zone objects from this set. The six objects were a 14-cm-wide wooden post, a 0.6-m-diameter hole in the soil, a 0.6-m basaltic rock, a cinder block, a stack of adobe bricks (front aspect), and a stack of adobe bricks (top aspect). Because radiometric contrast is a function of incidence angle due to the strong gradation of sky temperature, the imager was elevated to a height of 3 m above ground level to simulate an anticipated helicopter approach angle of ~25°. Horizontal polarization root-sum-squared (RSS) target-to-background contrasts ranged from 15–28 K, while vertical polarization RSS contrasts ranged from 3–10 K.
- An E-field polarized parallel to the horizon (H-polarization) presents far better temperature contrast than the orthogonal V-polarization. This effect is due primarily to the significantly higher reflection coefficient of packed dirt to the parallel polarization state, which provides lower background temperatures due to the effective cold sky temperatures (15).

3.3 Scenario C: Concealed Weapon Detection/Identification

Due to the general requirements to detect and/or identify concealed weapons carried by people at substantial (safe) standoff distances using imaging equipment with reasonably small aperture sizes, it is assumed that imaging systems designed for this scenario would most likely operate in the SMMW/THz regime, probably in one of the 320- or 640-GHz atmospheric transmission windows (see figure 2).

From table 2, the primary contrast mechanism for the listed targets against a human skin background near 500 GHz is emissivity. Assuming that the target and background are at the same temperature, the (target-to-background) contrast will occur due to the differences in emissivities:

- The estimated CR for a metal weapon against human skin is $\frac{0.91-0.00}{0.91+0.00} = 1$,
- The estimated CR for an explosive pack against human skin is $\frac{0.95-0.91}{0.95+0.91} = 0.02$.

Applying the CR for the case of an explosive pack against human skin at a temperature of approximately 310 K yields an equivalent blackbody temperature difference of approximately $310 \text{ K} \times 0.02 = 6.2 \text{ K}$.

4. Imaging System Requirements

An imaging system must meet resolution requirements to allow for enough spatial cycles on target at a desired standoff distance to enable an observer to adequately perform the task of either detecting or identifying a target against typical background materials. In addition, such a system must be capable of capturing image frames with enough SNR to produce good imagery at video frame rates.

The differential power received by the imaging system's receiver from the target and background is primarily governed by phenomenology. It is also affected by some of the imaging system characteristics/parameters such as the spectral bandwidth, the aperture size, and the instantaneous field of view (IFOV) of the imaging system. As such, realizing an adequate system SNR depends on achieving adequate system sensitivity (low noise-equivalent power [NEP]). To determine the required system sensitivity for capturing useful imagery at video rates, a radiometric formulation of the target and background powers received by the system's detector element(s) is first described.

Using the radiometric transfer process developed by Murrill et al. (16), the power emitted from the target and background surfaces within the detector area (in object space) and within the receiver spectral bandwidth is first calculated, and then these powers are propagated through any target concealment/obscurant material and through the atmosphere to the receiver aperture a distance R (meters) away (figure 8). The emitted powers are assumed to radiate in a Lambertian fashion (*Gain* equal to 4).

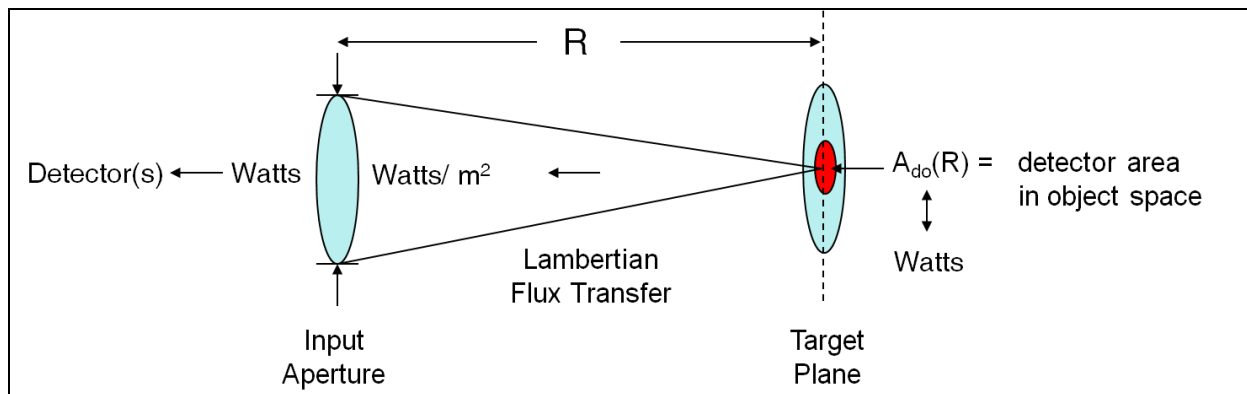


Figure 8. Illustration of the radiometric model for passive target/background thermal emission.

Calculation of the power emitted from the target/background surface begins with the calculation of thermal exitance by integrating the spectral exitance (Planck's radiation law [17]) over the spectral bandwidth of the system receiver and then multiplying by the emissivity of the surface. The thermal exitance (M) of the target or background surface is given by

$$M_{thermal} = \int_{\lambda_C - \Delta\lambda/2}^{\lambda_C + \Delta\lambda/2} \left(\frac{2\pi \times h \times c^2}{\lambda^5 \times (\exp\{h \times c / (\lambda \times k \times T)\} - 1)} \right) d\lambda \text{ in W/m}^2, \quad (6)$$

where h is Planck's constant (J·s), c is the speed of light (m/s), λ is wavelength (m), k is Boltzmann's constant (J/K), T is the surface temperature (K), λ_C is the center wavelength of the system receiver (m), and $\Delta\lambda$ is the spectral bandwidth of the system receiver (m).

The power emitted from the target/background surface into the detector's IFOV is calculated from

$$P_{emitted} = M_{thermal} \times A_{do}(R) \times \varepsilon_{surface} \text{ in W}, \quad (7)$$

where $A_{do}(R)$, the detector area in object space, is as calculated in equation 8 and $\varepsilon_{surface}$ is the emissivity of the surface.

The detector area, $A_{do}(R)$, is the detector area in object space and is given by

$$A_{do}(R) = \pi \left(\frac{IFOV}{2} \times R \right)^2 \text{ in m}^2, \quad (8)$$

where $IFOV$ is the detector's IFOV.

The emitted power from the target and background surfaces is then propagated to the imaging system through any target concealment/obscurant material and through the atmosphere to the receiver aperture located a distance R away, and the receiver aperture irradiance is calculated. The irradiance at the receiver aperture is given by

$$E_{aperture} = \frac{P_{emitted} \times \tau_{atm} \times \tau_{obsc}}{4\pi R^2} \times Gain \text{ in W/m}^2, \quad (9)$$

where $Gain$ is the reflective (emissive) gain from the target or background surface given by

$$Gain = \frac{4\pi}{\Omega_{refl}}, \quad (10)$$

and Ω_{refl} is the solid angle of the reflected (emitted) beam in steradians. For Lambertian emission, Ω_{refl} is π steradians, yielding a $Gain$ equal to 4.

Finally, the power incident on the detector is calculated to be

$$P_{det_IFOV} = E_{aperture} \times A_{aperture} \times \tau_{aperture} \times \eta_{antenna} \text{ in W}, \quad (11)$$

where $A_{aperture}$ is the area of the aperture in m^2 , $\tau_{aperture}$ is the transmission of the aperture, and $\eta_{antenna}$ is the coupling efficiency of the detector's antenna.

Combining equations 6–10 into equation 11 yields

$$P_{det_IFOV} = M_{thermal}(\lambda_c, \Delta\lambda, T) \times \epsilon_{surface} \times \left(\frac{IFOV}{2} \right)^2 \times A_{aperture} \times \tau_{atm} \times \tau_{obsc} \times \tau_{aperture} \times \eta_{antenna} \text{ in W. (12)}$$

Note that the power received by the system detector(s) is independent of range (R) (for ranges where the target is fully resolved). This is due to the fact that the surface area of the target or background that the system's IFOV subtends increases by R^2 as range increases, while the power density (irradiance) that the system aperture receives decreases by R^2 as range increases.

The power received by the system detector(s) is a strong function of the frequency or wavelength of the EM radiation along with the spectral bandwidth. Figure 9 shows the spectral exitance (M) of a blackbody at a temperature of 300 K as a function of wavelength. Note that radiant power peaks at a wavelength of approximately 10 μm (IR regime) and is approximately 7 orders of magnitude lower at a wavelength of 1 mm (MMW regime). Figure 10 displays this same curve on a log-log scale.

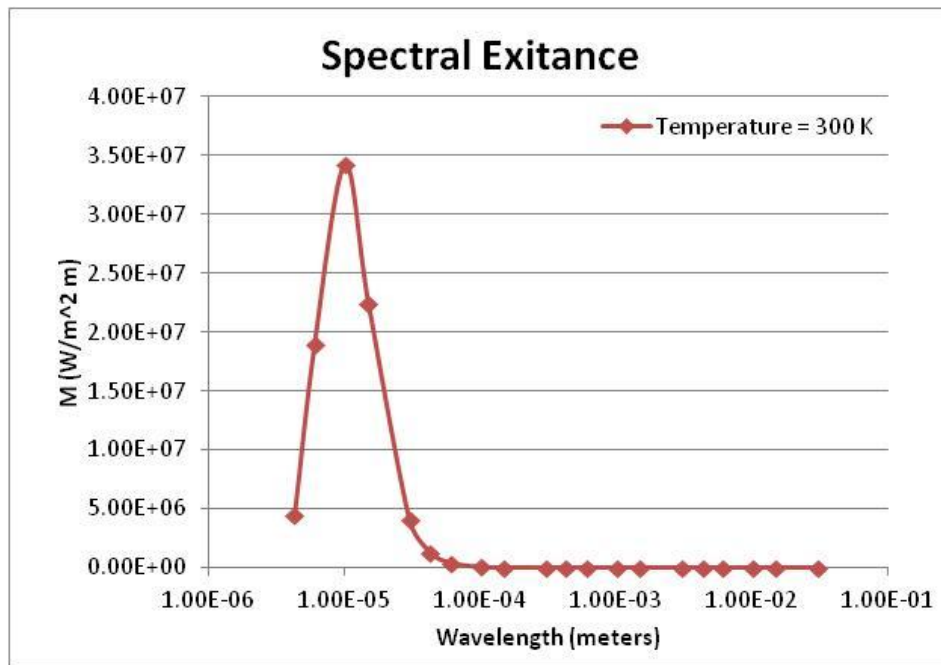


Figure 9. Spectral exitance of a blackbody at a temperature of 300 K.

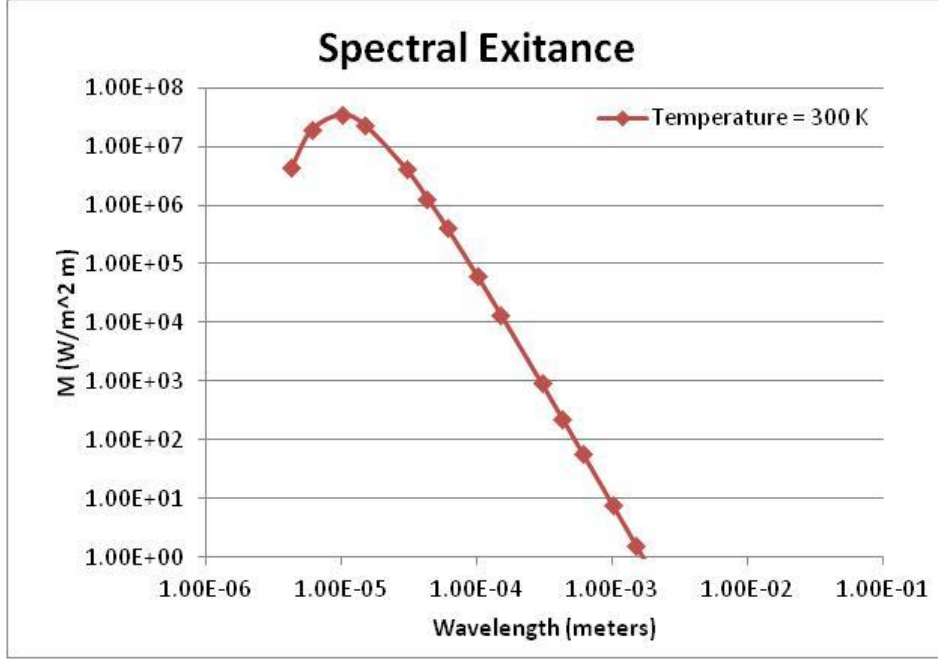


Figure 10. Spectral exitance of a blackbody at a temperature of 300 K plotted on a log-log scale.

The incremental temperature above a background temperature that produces a system SNR of unity is the system's noise equivalent difference temperature (NEDT) (18). For this analysis, the difference between the power received by the system detector(s) from the *target* surface and the power received from the *background* surface (from the minimum target-to-background apparent temperature difference) is equated to the system's electrical NEP such that the system SNR is unity, i.e.,

$$SNR_{System} = \frac{|P_{Tgt}(W) - P_{Bkgd}(W)|}{NEP_{System}}, \quad (13)$$

where $P_{Tgt}(W)$ is the power (in watts) received by the system detector(s) from the *target* surface (from equation 12), $P_{Bkgd}(W)$ is the power (in watts) received by the system detector(s) from the *background* surface (from equation 12), and NEP_{System} is the NEP of the system (in watts).

The system NEP is a function of the noise equivalent bandwidth (NEBW) and is given by

$$NEP_{System} = NEP^* \left(W / \sqrt{Hz} \right) \times \sqrt{NEBW (Hz)}, \quad (14)$$

where $NEP^* \left(W / \sqrt{Hz} \right)$ is the fundamental system sensitivity expressed as watts per root Hz, and NEBW (Hz) is inversely related to the detector temporal integration time (t_{det_int}) available for each image pixel per image frame (18, 19) by,

$$NEBW (Hz) = \frac{1}{2t_{det_int}(s)}. \quad (15)$$

Substituting equation 13 into equation 14 yields

$$NEP^* \left(W / \sqrt{Hz} \right) = \frac{|P_{Tgt}(W) - P_{Bkgd}(W)|}{(SNR_{System} \times \sqrt{NEBW (Hz)})} \cdot (W \cdot Hz^{-1/2}) \quad (16)$$

where again $P_{Tgt}(W)$ is the power (in watts) received by the system detector(s) from the *target* surface (from equation 12), $P_{Bkgd}(W)$ is the power (in watts) received by the system detector(s) from the *background* surface (from equation 12), and NEBW (Hz) is the noise equivalent bandwidth of the system.

Alternatively, substituting equation 15 into equation 16 yields

$$NEP^* \left(W / \sqrt{Hz} \right) = \frac{|P_{Tgt}(W) - P_{Bkgd}(W)|}{SNR_{System}} \times \sqrt{2t_{det_int}(s)} \cdot (W \cdot Hz^{-1/2}) \quad (17)$$

The previous section provided minimum contrast temperature differences that an imaging system must be capable of capturing, with adequate SNR, for three important MMW and/or SMMW/THz imaging scenarios. Within each scenario, the worst-case contrast temperature differences were 2 and 6 K at 77 GHz, and approximately 6 K at 320 or 640 GHz.

From a top level, imaging systems designed to effectively image in these scenarios must be able to capture images with 2–6 K contrast temperature differences in the respective EM radiation frequency bands with adequate SNR (assume at least an SNR = 6) under the very crucial constraint of operating at video rates (approximately 30 Hz).

As can be seen from the above formulations, many factors go into determining the differential power levels actually captured by the system receiver element(s), which then, of course, drive the system noise floor or sensitivity requirement. To summarize, the primary factors are the following:

- the effective exitance (power) levels of the target and background contained within the spectral bandwidth of the system (includes target and background temperatures and emissivities),
- the minimum contrast temperature difference that must be resolved,
- the IFOV of the system,
- the size of the receiver aperture,
- the atmospheric attenuation at standoff range,
- the coupling efficiency of the receiver/antenna, and
- any concealment material attenuation.

Again, on the system receiver side of the equation (system noise), a crucial parameter is the amount of integration time available for each image pixel per image frame. The NEP* sensitivity

requirement of the system scales with the square root of the available integration time ($t_{\text{det_int}}$) — System noise (watts) = NEP* (watts per root Hz)/square root of $2t_{\text{det_int}}$ (s). The less integration time available to the system, the higher the imaging system sensitivity requirement (lower numerical value).

All of the above factors have been incorporated into and accounted for in the U.S. Army Research Laboratory's (ARL) Enhanced Terahertz/MMW Imaging System Performance Analysis and Design Tool for Concealed Weapon Identification (20). Present plans call for evaluating select passive MMW and SMMW/THz imaging systems using this modeling tool.

5. Discussion and Conclusions

Phenomenologically, the advantages of *passive* imaging in the MMW regime include the following:

- Low atmospheric attenuation and scattering
- Low attenuation due to atmospheric fog, smoke, dust, sand, and typical person-borne concealment materials.

Relative to *passive* imaging in the SMMW/THz regime, the primary disadvantage of *passive* imaging in the MMW regime is lower spatial resolution for a given imaging system aperture size. A secondary disadvantage is the relative dependence on sky illumination for larger target-to-background CRs.

Advantages of passive imaging in the SMMW/THz regime include the following:

- Increased spatial resolution for a given imaging system aperture size
- Slightly better target-to-background CRs with indoor scenarios (no sky illumination) due to higher thermal emissivities and spectral exitances.

Relative to *passive* imaging in the MMW regime, the primary disadvantages of *passive* imaging in the SMMW/THz regime include the following:

- Higher atmospheric attenuation and scattering
- Higher attenuation due to atmospheric fog, smoke, dust, sand, and typical person-borne concealment materials
- Possible degradation of image quality (lower SNCRs) due to clutter from spatial variations in atmospheric attenuation and spatial/temporal variations in concealment material attenuation due to material motion relative to the target/background.

Some knowledge gaps remain in the understanding/quantification of a few phenomenological aspects of passive imaging in the MMW and SMMW/THz regimes. For the most part, these knowledge gaps fall into the category of clutter and include the following:

- A better understanding of the impact of variations in both sky and fog illumination on an observer's ability to perform the task of detecting or identifying a slightly cluttered target within a slightly cluttered background
- A better, more quantitative understanding of the impact of spatial variations of atmospheric attenuation on an observer's ability to perform the task of detecting or identifying a slightly cluttered target within a slightly cluttered background
- A better, more quantitative understanding of the impact of variations in concealment material attenuation due to material motion relative to the target/background on an observer's ability to perform the task of detecting or identifying a slightly cluttered target within a slightly cluttered background.

Based on the MMW and SMMW/THz radiometric data cited in the imaging scenarios of section 3, along with an assumption that a reasonable SNR of 6 (approximately 8 dB) is required for good imagery, it is concluded that the following minimum imaging system receiver sensitivities are required for the successful discrimination of all targets of interest within their respective backgrounds:

- In-flight obstacle avoidance: $2 K/6 =$ approximately 0.3 K
- Landing/takeoff obstacle avoidance: $6 K/6 =$ approximately 1.0 K
- Concealed weapon detection/identification: $6.2 K/6 =$ approximately 1.0 K.

The extremely important constraint that goes along with these sensitivity levels is the requirement for the *passive* MMW and/or SMMW/THz system to meet these specifications using real-time, video frame rates.

If, for example, a *passive* MMW or SMMW/THz imaging system uses a scanning, line-array receiver architecture, then the receiver sensitivity requirement — $NEP^*(\text{watts per root Hz})$ — will nominally increase relative to a system using a FPA by the square-root of the number of rows or columns that are scanned to form a complete image. (This assumes a zero-time budget for the scanning process itself.) If a *passive* MMW or SMMW/THz imaging system uses a single-pixel, scanning receiver architecture, then the receiver sensitivity requirement — $NEP^*(\text{watts per root Hz})$ — will nominally increase relative to a system using a FPA by the square-root of the number of pixels that are scanned to form a complete image. (Again, this assumes a zero-time budget for the scanning process.)

Mathematical formulations of the required passive imaging system receiver sensitivity requirement — $NEP^*(\text{watts per root Hz})$ — to provide image frames with enough SNR to

produce good imagery at video frame rates have been derived (equations 16 and 17). The equations show that the required system sensitivity is a function of the following variables:

- the spectral bandwidth of the imaging system,
- the minimum temperature difference between the target and the background,
- the emissivities of the target and background,
- the IFOV of the system detector(s),
- the area of the system entrance aperture,
- atmospheric transmission (attenuation),
- aperture transmission,
- obscurant transmission (attenuation),
- antenna coupling efficiency,
- the desired system SNR, and
- the available detector integration time per pixel per frame.

Future work will include identifying and subsequent performance modeling of selected commercial-off-the-shelf (COTS) and/or Government off-the-shelf (GOTS) MMW and/or SMMW/THz passive imaging systems. These systems will be analyzed using ARL's Enhanced Terahertz Imaging System Performance Analysis and Design Tool for Concealed Weapon Identification (20).

6. References

1. Rosker, M. J.; Wallace, H. B. Imaging Through the Atmosphere at Terahertz Frequencies. *Microwave Symposium 2007*, IEEE/MTT-S International, 773–776.
2. Appleby, R.; Wallace, H. B. Standoff Detection of Weapons and Contraband in the 100 GHz to 1 THz Region. *Antennas and Propagation, IEEE Transactions* **Nov. 2007**, 55 (11), 2944–2956.
3. Wallace, H. B. Atmospheric Phenomenology in the 10 to 10000 GHz Spectral Region. *4th International Aviation Security Technology Symposium*, Nov. 2006.
4. Wikner, D. Millimeter-wave Propagation Through a Controlled Dust Environment. *Proc. SPIE 6548, Passive Millimeter-Wave Imaging Technology X*, 654803, May 2007.
5. Schuetz, C. A.; Stein, E. L., Jr.; Samluk, J.; Mackrides, D.; Wilson, J. P.; Martin, R. D.; Dillon, T. E.; Prather, D. W. Studies of Millimeter-wave Phenomenology for Helicopter Brownout Mitigation. *Proc. SPIE 7485, Millimetre Wave and Terahertz Sensors and Technology II*, 74850F, September 2009.
6. Mackrides, D. G.; Schuetz, C. A.; Martin, R. D.; Dillon, T. E.; Yao, P.; Prather, D. W. Progress Toward a Video-rate, Passive Millimeter-wave Imager for Brownout Mitigation. *Proc. SPIE 8022, Passive Millimeter-Wave Imaging Technology XIV*, 802203, May 2011.
7. Bjarnason, J. E.; Chan, T.L.J.; Lee, A.W.M.; Celis, M. A.; Brown, E. R. Millimeter-wave, Terahertz, and Mid-infrared Transmission Through Common Clothing. *Appl. Phys. Lett.* **July 2004**, 85, 519.
8. Petkie, D. T.; De Lucia, F. C.; Castro, C.; Helminger, P.; Jacobs, E. L.; Moyer, S. K.; Murrill, S.; Halford, C.; Griffin, S.; Franck, C. Active and Passive Millimeter- and Sub-millimeter-wave Imaging. *Proc. SPIE 5989, Technologies for Optical Countermeasures II; Femtosecond Phenomena II; and Passive Millimetre-Wave and Terahertz Imaging II*, 598918, November 2005.
9. Wikner, D. A. Analysis of Passive Millimeter-wave Imagery Texture for Enhanced Aircraft Obstacle Avoidance. *Proc. SPIE 5410, Radar Sensor Technology VIII and Passive Millimeter-Wave Imaging Technology VII*, p. 230, August 2004.
10. Sanchez-Marin, F. J. A New Method for Determining the Emissivity of the Human Skin in Vivo. *Bioinformatics and Biomedical Engineering (iCBBE), 2010 4th International Conference on* **June 2010**, 1–3, 18–20.

11. Hewison, T. J. Airborne Measurements of Forest and Agricultural Land Surface Emissivity at Millimeter Wavelengths. *Geoscience and Remote Sensing. IEEE Transactions on* **Feb. 2001**, 39 (2), 393–400.
12. Boreman, G. D. *Basic Electro-Optics for Electrical Engineers*; Chapter 2, SPIE Optical Engineering Press: Bellingham, 1998.
13. Wikner, D. A. Analysis of Passive Millimeter-wave Imagery Texture for Enhanced Aircraft Obstacle Avoidance. *Proc. SPIE 5410, Radar Sensor Technology VIII and Passive Millimeter-Wave Imaging Technology VII*, p. 230, August 2004.
14. Wikner, David A. Passive Millimeter-wave Imagery of Helicopter Obstacles in a Sand Environment. *Proc. SPIE 6211, Passive Millimeter-Wave Imaging Technology IX*, 621103, May 2006.
15. Schuetz, C. A.; Stein, E. L. Jr.; Samluk, J.; Mackrides, D.; Wilson, J. P.; Martin, R. D.; Dillon, T. E.; Prather, D. W. Studies of Millimeter-wave Phenomenology for Helicopter Brownout Mitigation. *Proc. SPIE 7485, Millimetre Wave and Terahertz Sensors and Technology II*, 74850F, September 2009.
16. Murrill, S.; Redman, B.; Espinola, R.; Franck, C.; Petkie, D.; De Lucia, F.; Jacobs, E.; Griffin, S.; Halford, C.; Reynolds, J. Advanced Terahertz Imaging System Performance Model for Concealed Weapon Identification. (Invited Paper), *Proc. SPIE*, 6549, 654902-1, 2007.
17. Hecht, E. *Optics*; (Third Edition), Chapter 13, Addison-Wesley: Reading, 1998.
18. Holst, G. *Electro-Optical Imaging System Performance*; Chapter 18, SPIE Optical Engineering Press: Bellingham, 1995.
19. Boreman, G. D. *Basic Electro-Optics for Electrical Engineers*; Chapter 5, SPIE Optical Engineering Press: Bellingham, 1998.
20. Murrill, S. R.; Franck, C. C.; Espinola, R. L.; Petkie, D. T.; De Lucia, F. C.; Jacobs, E. L. Enhanced Terahertz Imaging System Performance Analysis and Design Tool for Concealed Weapon Identification. *Proc. SPIE 8188, Millimetre Wave and Terahertz Sensors and Technology IV*, 81880J, October 2011.

List of Symbols, Abbreviations, and Acronyms

ARL	U.S. Army Research Laboratory
CRs	contrast ratios
CW	continuous-wave
DVEs	degraded visual environments
EM	electromagnetic
FPA	focal-plane-array
IFOV	instantaneous field-of-view
IR	infrared
MMW	millimeter-wave
NEDT	noise equivalent difference temperature
NEP	noise-equivalent power
RSS	root-sum-squared
SCRs	signal (target)-to-clutter ratios
SMMW	submillimeter-wave
SNCRs	signal-to-noise plus clutter ratios
SNRs	signal-to-noise ratios
THz	terahertz

1 ADMNSTR
(PDF) DEFNS TECHL INFO CTR
ATTN DTIC OCP

5 US ARMY RSRCH LAB
(PDF) ATTN RDRL CIO LL TECHL LIB
10 ATTN RDRL SEE E
(HCS) S MURRILL (10 HCS + 1 PDF)
G WOOD
L BLISS
RDRL-SEE-O
P PELLEGRINO